

NON-DESTRUCTIVE IR INSPECTION OF DRY MULTILAYER CARBON AND GLASS FIBRE PREFORMS

Ocana, J^{1*}, Robitaille, F¹

¹ Department of Mechanical Engineering,
University of Ottawa, Ottawa, Canada

* Corresponding author (jmart228@uottawa.ca)

Keywords: *IR inspection, carbon and glass fibre preforms*

Carbon and glass fibre composites are increasingly used in many industries including aerospace and defence because of their advantageous stiffness- and strength-to-weight ratios. Out-of-autoclave liquid moulding processes whereby a liquid resin is infused in a dry carbon or glass fibre textile preform prior to curing are displacing prepreg-based in-autoclave consolidation processes on the grounds of favourable manufacturing flexibility and costs. However, realizing the advantages made possible by liquid moulding processes for manufacturing reproducible high-performance parts and structures that may compete with those manufactured using established techniques requires the use of advanced carbon and glass fibre preforms that are precisely engineered and manufactured as assembled units, as opposed to loose pieces of thin reinforcement fabrics laid manually over moulds. Just as composite parts are inspected on a routine basis, inspecting such textile preforms prior to resin infusion holds the promise of reducing part rejection rates and overall costs in a production context. However, whilst the inspection of composite parts is well established, no prior work was reported on the inspection of dry preforms. This work describes the use of thermography for non-destructive inspection (NDI) of dry carbon and glass fibre preforms, aiming at identifying defects in thick preforms made of industrial carbon and glass fibre textile reinforcements that cannot be observed by visual inspection. The preforms tested contained two or four layers of textiles with different architectures. Individual layers featured defects of different types, orientations, depths and configurations. Infrared (IR) images were analysed using MATLAB 7.0. Results show that defects were identified successfully. The results also show the sensitivity of the technique to the above parameters, in terms of how they may promote or hinder defect detection.

1 INTRODUCTION

Carbon (CF) and glass fibre (GF) composites have seen increased use due to their specific properties combining high strength and low density [1]. Two major manufacturing routes are available for manufacturing glass and carbon fibre composites, prepreg-based and out-of-autoclave liquid moulding (LM) processes. LM processes enable low cost combined with high manufacturing flexibility when compared with prepreg-based routes. However, LM processes still require improvements in reliability and consistency. Reinforcement fibre beds are often built from separate pieces of textile layers that are laid manually over moulds, increasing costs significantly whilst reducing reproducibility [2-4]. Literature has reported on studies towards the development of automated lay-up systems [5-7] but required lay-up rates of 400Kg/hr [6] remain elusive. Due to the possible defects that can occur upon textile lay-up, even automated systems face issues of reproducibility and consistency [2-4].

Implementing in-situ, fast, non-destructive inspection of preforms during or after lay-up could offer an alternative approach to improving preform reproducibility through process diagnosis and reducing part rejection rates, avoiding badly manufactured consolidated parts [5]. Among the four major non-destructive inspection methods namely infrared (IR) thermography, ultrasonic scanning, shearography and laser ultrasound [8-12], IR is largely used for the inspection of consolidated carbon and glass fibre composites as it enables coverage of large areas over short periods of time [8]. Numerous papers report on IR inspection including passive, active, and cycled approaches combined with different heating sources, all applied to consolidated composites [9,13,14].

The literature reports axial thermal conductivities ranging from 7 to 10 W/mK for PAN-based carbon fibres and 1.2 to 1.35 W/mK for E-glass fibres [15,16]. As preforms are not consolidated solids and fibres are often thermally anisotropic (i.e. axial conductivity 5 to 10 times higher than radial conductivity) [17,18], thermal properties of the textiles may play an important role in the identification of defects. Yang et al. [19,20] proved the influence of interactions between fibres on the in-plane and through-thickness thermal conductivities of textiles. According to Bol'shakova et al. [21] multiple fibre contacts tend to reduce the thermal anisotropy of textiles.

The literature features numerous studies reporting on the non-destructive inspection of glass and carbon fibre composites, but the identification of defects in dry glass and carbon preforms is poorly reported. This paper investigates the potential of IR thermography for identifying defects in dry multilayer GF and CF preforms. Two textiles were selected for constructing GF and CF samples, some featuring defects and some being defect free. The samples were probed using active thermography with different heat sources. Thermographs were processed in MATLAB 7.0 and defects were identified as reported below.

2 MATERIALS AND EXPERIMENTAL METHODS

All samples were held vertically using 2 pieces of light thermoplastic thread, under a cover and between a heating source – either a 500 W halogen lamp for carbon fibre samples or a 1800 W heating blower for glass fibre samples – mounted behind them and a FLIR i7 infrared (IR) camera on their front side. Both heating techniques were used as part of ongoing efforts towards transitioning the inspection method to an industrial setting. The first and last layers in stacking sequences were exposed to the IR camera and heating source, respectively. The IR camera was positioned 100 mm from samples, covering approximately 50% of total sample area. Defects were created in the last layer by removing or cutting yarns as detailed below.

The heating source was turned on until a target temperature at the centre of thermographs was reached. Target temperatures ranged between 45°C and 60°C depending on the textile; temperatures that returned the best contrasts were selected for each textile. Thermographs were captured every 5 seconds during both heating and cooling phases; upon cooling the heating source was always masked. The emissivity constants adopted for all glass and carbon fibre samples were 0.75 and 0.90 respectively; the constants did not affect detection capability.

Three repeats were performed on each sample; a minimum delay of 300 seconds between experiments was used to ensure thermal equilibrium in cooled samples. All repeats presented similar responses; only one repeat was retained for analysis in all cases.

2.1 Glass Fibre Samples – Satin and Twill

All glass fibre samples were made of 2 E-glass Texonic textiles: a 297 g/m² Satin 8 (STG) and a 315 g/m² 2x2 balanced twill (TWG). STG featured 1K yarns while TWG featured 3K yarns. 10 cm x 10 cm samples featuring 2 or 4 plies stacked in different sequences were made for each textile. Layers were glued using Airtec2 spray adhesive and samples were compacted under 4.6 KPa for 300 seconds. Sample details appear in Table 1. Five defect-free samples and five samples featuring defects were made for both STG and TWG textiles. Yarns extend along 2 orientations in each ply namely 0/90° or ±45°. Defects were created by removing 1 or 3 groups of 1 to 3 yarns along the horizontal in the last layer. For samples featuring 3 groups of defects, 3 yarns remained between each defect. The 1800 W blower was positioned at 600 mm from the back side of glass fibre samples. Target temperatures were 45°C and 40°C for all 2 and all 4 layer samples, respectively.

2.2 Carbon Fibre Samples – Twill and Unidirectional-Stitched

All carbon fibre samples were made from two Texonic textiles: a 215 g/m² 2x2 balanced twill weave (TWC) and a 285 g/m² unidirectional stitched fabric (USC). All textiles were made from Toho Tenax HTS40 fibers. TWC featured 3K yarns while USC featured 12K yarns. 10 cm x 10 cm samples featuring 2 or 4 plies stacked in

NON-DESTRUCTIVE IR INSPECTION OF DRY MULTILAYER CARBON AND GLASS FIBRE PREFORMS

different sequences were made for each textile. Layers were glued using Airtec2 spray adhesive and samples were compacted under 4.6 KPa for 300 seconds. Sample details appear in Tables 1 and 2 for TWC and USC respectively. Five defect-free samples and five samples featuring defects for TWC and USC samples.

Defects in TWC samples were created by removing 1 or 3 groups of 1 to 3 yarns along the horizontal in the last layer; 3 yarns remained between each defect for TWC samples featuring 3 groups of missing yarns. Meanwhile, USC samples featured 2 types of defects, parallel or perpendicular to the orientation of yarns in the last layer. Parallel and perpendicular defects were created either by cutting stitches to enable the removal of yarns, or by cutting yarns, respectively. Defect widths were equivalent to removing $\frac{1}{2}$, 1 or 2 yarns. Defects were separated by the width of 2 yarns in samples featuring multiple defects. The 500 W halogen lamp was positioned at 350 mm for all TWC samples and at 450 mm for all USC samples. Target temperatures were 60°C and 50°C for TWC and USC samples respectively.

Sample			Orientation of layers (First to last layer)	Defect in the last layer (missing yarns)		
Glass	Carbon	One		Two	Three	
STG_01	TWG_01	TWC_01	[0/90°, 0/90°]			
STG_02	TWG_02	TWC_02	[0/90°, ±45°]			
STG_03	TWG_03	TWC_03	[±45°, 0/90°]			
STG_04	TWG_04	TWC_04	[±45°, ±45°]			
STG_05	TWG_05	TWC_05	[0/90°, 0/90°, 0/90°, 0/90°]			
STG_06	TWG_06	TWC_06	[0/90°, 0/90°]	↔		
STG_07	TWG_07	TWC_07	[0/90°, 0/90°]		↔	
STG_08	TWG_08	TWC_08	[0/90°, 0/90°]			↔
STG_09	TWG_09	TWC_09	[0/90°, 0/90°]	↔	↔	↔
STG_10	TWG_10	TWC_10	[0/90°, 0/90°, 0/90°, 0/90°]	↔	↔	↔

Table 1. Description of STG, TWG and TWC samples. Defects: ↔ defect along horizontal (0°)

Sample	Orientation of layers (First to last layer)	Defect in the last layer (missing yarns)		
Carbon		One	Two	Three
USC_01	[0°, 0°]			
USC_02	[0°, 90°]			
USC_03	[90°, 0°]			
USC_04	[90°, 90°]			
USC_05	[0°, 0°, 0°, 0°]			
USC_06	[0°, 0°]	↔		
USC_07	[90°, 0°]	↔		
USC_08	[90°, 90°]	↔		
USC_09	[90°, 90°]	↕	↕	↕
USC_10	[0°, 0°, 0°, 0°]	↕	↕	↕

Table 2. Description of USC samples. Defects: ↔ defect along horizontal (0°) and ↕ defect along vertical (90°)

2.3 Analysis

The aim of analysis was to perform a comparison between actual (AD) and identified defect areas (ID) in thermographs. Thermographs were converted into temperature maps (T_m); a MATLAB code identified the maximum and minimum temperatures on thermographs, converting colour thermograph scales into numerical temperature scales. Then, a Fast Fourier Surface Transform (FFST) was performed on data to compute a Discrete Fourier Transform (DFT). Results were expressed as temperature matrices (TM). DFT was determined using Eq 1 where n represents frequency magnitudes, x and y map coordinates, and L_x, L_y are map lengths; here $n = 10$, and $L_x = L_y$.

$$TM(j, k) = \frac{1}{L_x L_y} \sum_{j=1}^n \sum_{k=1}^n T_m(x, y) \cdot |[T_m]|_{max} \cdot \sin\left(\frac{(2jx + 1)\pi}{4L_x}\right) \cdot \sin\left(\frac{(2ky + 1)\pi}{4L_y}\right) \quad (1)$$

2.3.1 Glass Fibre Samples (STG and TWG)

The effects of temperature changes over time were investigated, analysing defect-free zones and defect points in TMs for GF samples as shown in Figure 1 for sample STG_08. TMs were associated with a time t_i from start of heating to end of cooling. Better contrast between defects and defect-free zones were noted in TMs at the beginning of heating and cooling phases, i.e. within 20 seconds. Best contrast was achieved at 15 seconds after turning off the heating blower; this paper focuses on these results for GF samples.

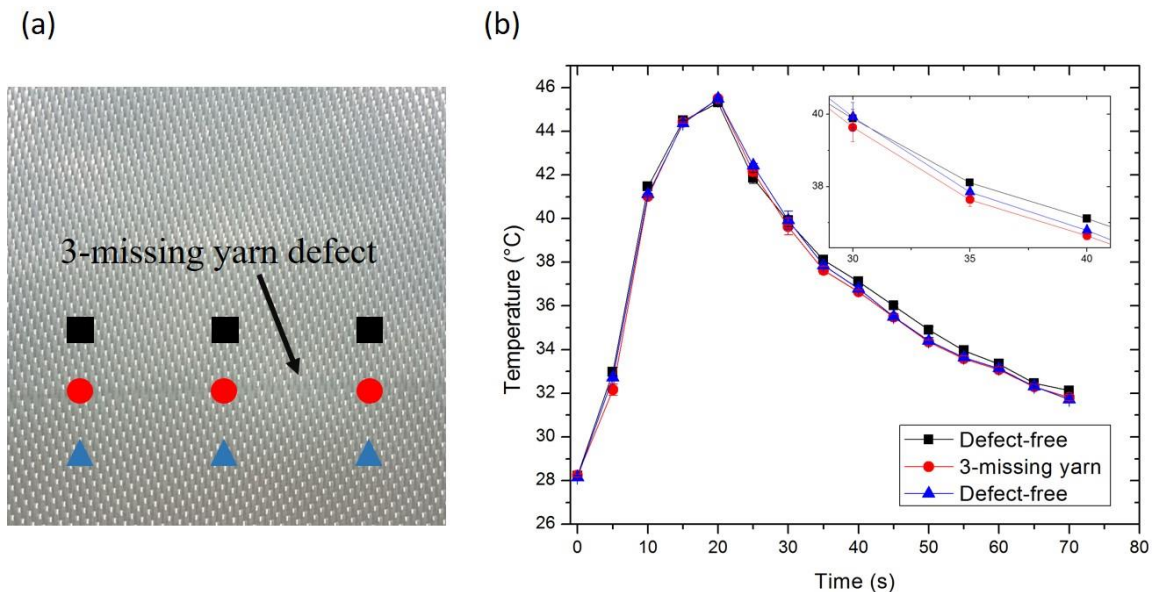


Figure 1. Sample STG_08 (a) back of sample STG_08, black squares and blue triangles indicate defect-free points while red circles indicate 3-missing-yarn defects; (b) tracking the average temperature values at points represented by squares, triangles, and circles in TMs.

2.3.2 Carbon Fibre Samples (TWC and USC)

Here again the effects of temperature changes over time were investigated, analysing defect-free zones and defect points in TMs for CF samples. TMs were associated with a time t_i from start of heating to end of cooling. Defects were better noticed in TMs related to thermal transitions, i.e. room temperature to heating and heating to cooling. A MATLAB function created a series of $n - 1$ time-contrast matrices (CM), each containing differences between temperatures recorded at times t_{i+1} and t_i with $0 \leq i \leq n - 1$. These temperature differences were obtained by subtracting entries of matrices TM at times t_{i+1} and t_i as shown in Eq 2.

$$[CM]_i = [TM]_{i+1} - [TM]_i \quad (2)$$

Since results were better noticed in thermal transitions, these transitions were labelled as H_tCM (heating transition contrast matrices) and C_tCM (cooling transition contrast matrices). Figure 2 shows how the contrast between defect-free zones and points featuring defects is enhanced using CMs for TWC_08. This paper focuses on C_tCM transitions recorded for carbon fibre samples.

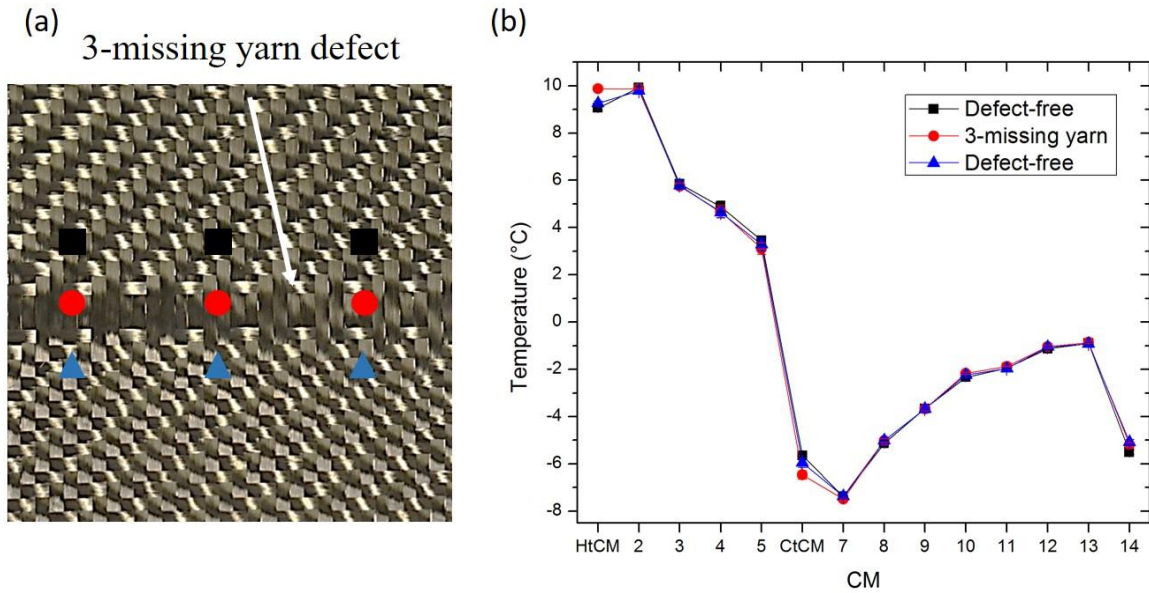


Figure 2. Sample TWC_08 (a) back of sample TWC_08, black squares and blue triangles indicate defect-free points while red circles 3-missing-yarn defects; (b) tracking the average temperature values at points represented by squares, triangles, and circles in CMs.

2.3.3 Defect Identification

TMs and CMs were evaluated by dividing samples into defect-free zones and zones featuring defect(s), identifying possible defect locations and IDs. The analyses were performed applying 2nd, 3rd, 6th degree fitted curves. In preliminary work, defects were identified as valleys or hills in TMs and CMs; defect-free samples featured a gently concave temperature distribution. Then, a 3rd degree polynomial curve was used in eliminating defect-free samples and in identifying the presence of one defect. A 6th degree polynomial curve was used in identifying up to three defects. The latter evaluates IDs by optimizing R-squared values.

3 RESULTS

3.1 STG samples

No defects were identified by the MATLAB code in thermographs nor in any HT generated from defect-free glass fibre satins. TMs from defect-free samples featured a generally concave shape featuring minimum temperature values at their periphery as shown in Figure 3 for sample STG_01. Results for STG samples appear in Table 3.

All defect locations and areas were identified for 2 layers STG samples featuring defects with the exception of 1- and 2-yarn defects in sample STG_09. For samples featuring only one defect, an increase in AD resulted in a similar increase in ID. STG_06 and STG_07 featured ADs of $1.0 \pm 0.3 \%$ and $2.0 \pm 0.5 \%$ compared with IDs of 11.81 % and 14.59 % respectively; IDs were considerable higher than ADs, possibly a result of the satin 8 pattern. For 2 layers sample STG_09 featuring three defects, only the 3-yarn defect was identified showing a possible interaction between defects due to heat transfer. Defects in 4 layers samples STG_10 were not identified.

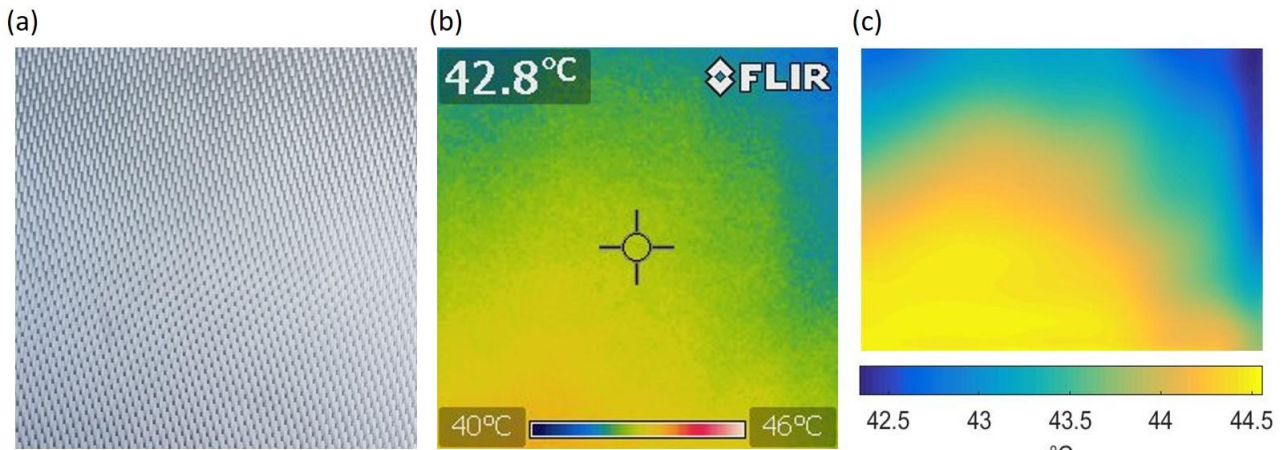


Figure 3. Results for defect-free sample STG_01 (a) front side of sample, (b) Thermograph taken at 15s, and (c) TM at 15s.

3.2 TWG samples

No defects were identified by the MATLAB code in thermographs nor in any HT generated from glass fibre twills, as reported above for STG samples. TMs from defect-free samples featured a generally concave shape featuring minimum temperature values at peripheries. Results for TWG samples also appear in Table 3.

All defect locations and areas were identified for 2 layers TWG samples featuring defects. For samples featuring only 1 defect, an increase in AD did not affect ID; samples TWG_06, TWG_07, and TWG_08 featured IDs equal to 11.54%, 11.79% and 10.73%, respectively. All 3 defects were identified for sample TWG_09 as shown in Figure 4; ID was higher than AD at 59.43% against 24.1%, which blended zones related to 1- and 2-yarn defects. The remaining 3 yarns between both defects did not provide sufficient contrast between zones featuring defects and defect-free zones of sample TWG_09. Defects were not identified for 4 layers samples.

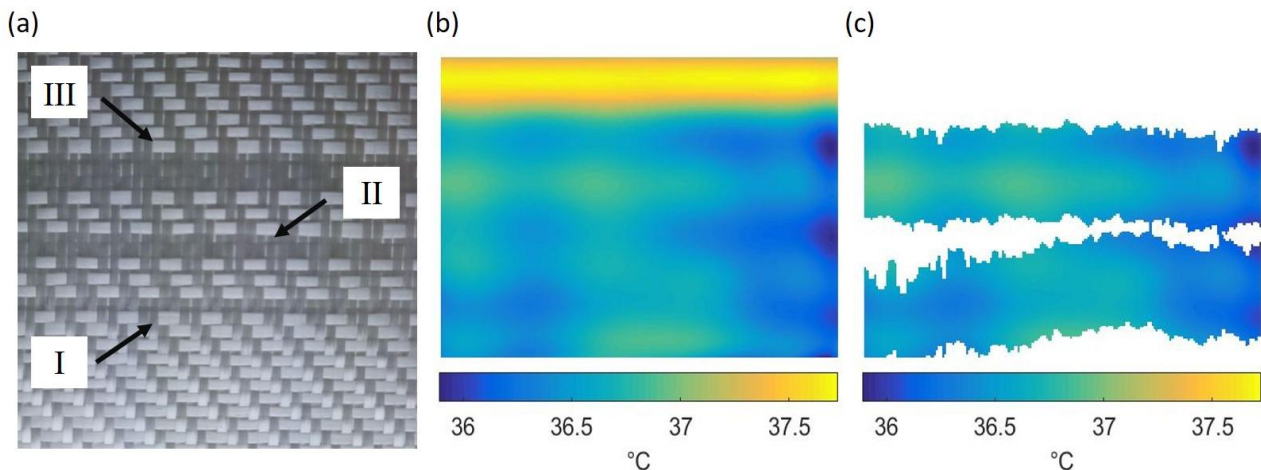


Figure 4. Sample TWG_09 featuring 3 defects, (a) back side of sample, (I) 1-missing (II) 2-missing, and (III) 3-missing yarn defects, (b) TM at 15s, and (c) defects identified.

<i>TM</i>	STG		<i>TM</i>	TWG	
	<i>AD (%)</i>	<i>ID (%)</i>		<i>AD (%)</i>	<i>ID (%)</i>
STG_06	1.0 ± 0.3	11.81	TWG_06	4.1 ± 0.4	11.54
STG_07	2.0 ± 0.5	12.69	TWG_07	6.5 ± 0.5	11.79
STG_08	2.3 ± 0.5	14.59	TWG_08	10.7 ± 0.3	10.73
STG_09	5.6 ± 1.6	10.39	TWG_09	24.1 ± 1.5	59.43
STG_10	5.2 ± 1.4	-	TWG_10	23.1 ± 1.3	-

Table 3. Results for STG and TWG glass fibre samples featuring defects

3.3 TWC samples

No defects were identified by the MATLAB code in thermographs nor in any C_tCM , in a behaviour similar to that observed in TMs for STG and TWG samples. C_tCM from defect free-samples featured a generally concave shape featuring minimum temperature values at their periphery. All defect-free samples returned a similar profile.

Results for TWC samples appear in Table 4. All defect locations and areas were identified for 2 layers TWC samples featuring defects, except for 1- and 2-yarn defects in sample TWC_09 where missing 1- and 2- yarns were identified as one single defect, Figure 5. For samples featuring only 1 defect, IDs were similar for 2- and 3-yarn defects; 12.3% and 12.0% for samples TWC_07 and TWC_08 respectively. A similar trend was observed for TWG samples. ID was 20.96% for TWC_09, slightly smaller than AD at $25.9 \pm 1.4\%$ but higher than both values for sample TWC_08. For sample TWC_10, only the 3-yarn defect was identified.

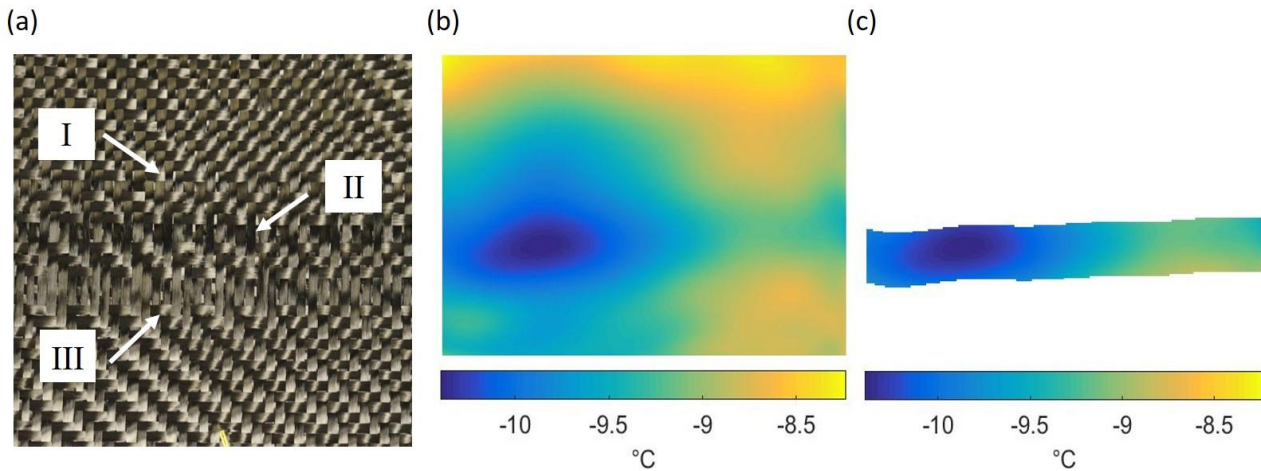


Figure 5. Sample TWC_09 featuring 3 defects, (a) back side of sample, (I) 1-missing (II) 2-missing, and (III) 3-missing yarn defects, (b) C_tCM , and (c) defects identified.

3.4 USC Samples

No defects were identified by the MATLAB code in thermographs nor in any C_tCM , as previously observed from results for STG, TWG and TWC samples. Profiles from other samples were slightly smoother than those from samples USC_01 and USC_03 which featured noise originating from stitch lines in the USC textile. C_tCM from defect-free USC samples featured a generally concave shape upon 3rd order fitting, featuring minimum temperature values at their periphery. Results for USC samples appear in Table 4.

IDs of 19.5%, 23.3% and 11.3% for samples USC_06 to USC_08 featuring only one defect were slightly higher or equal to ADs. All defect locations and areas were identified by the MATLAB code for samples USC featuring 3 defects, with IDs of 60.9% and 55.0% for samples USC_09 and USC_10 respectively.

C_t CM	TWC		C_t CM	USC	
	AD (%)	ID (%)		AD (%)	ID (%)
TWC_06	4.3 ± 0.5	-	USC_06	11.9 ± 0.2	19.50
TWC_07	8.8 ± 0.3	12.30	USC_07	12.3 ± 0.3	11.31
TWC_08	10.7 ± 0.4	11.95	USC_08	14.5 ± 0.3	31.56
TWC_09	25.9 ± 1.4	20.96	USC_09	42.2 ± 1.4	60.85
TWC_10	24.6 ± 1.3	11.61	USC_10	42.7 ± 1.5	55.02

Table 4. Results for TWC and USC carbon fibre samples featuring defects.

4 DISCUSSION

Defects were more prominent and quantified more accurately when a strong contrast was present between the defects and surrounding defect-free areas in thermographs. Strong contrast differences in TMs and C_t CMs over the corresponding zones facilitated identification. Contrast intensity depends on the thermal properties of fibres, yarns and preforms. Carbon is an excellent thermal conductor, allowing stronger contrasts between defect-free zones and zones featuring defects to appear within short time periods. Due to high heat dissipation rates, defects were better noticed on C_t CMs since the 5s time gap between thermographs was too long to capture significant contrasts. Conversely, glass as a thermal insulator provided better contrasts in thermographs taken up to at 15s after the heat source was turned off, due to lower heat dissipation rates.

Experimental data points to textile type having a major effect of results. A comparison between samples TWG_08 and TWC_08 shows similar ID values at 10.73% and 11.85% respectively. TWC and TWG samples presented similar ID values; meanwhile, STG samples featured a direct relationship between AD and ID.

USC samples showed an influence of yarn patterns which was not observed clearly from data for woven samples due to interlacing and multiple contacts between yarns at crossovers that create complex paths for heat transfer. When yarns featured similar orientations in stacking sequences as seen for example in samples USC_06 and USC_07, ID was higher than AD. When defects were perpendicular to yarn orientations in both layers, say in sample USC_08, AD was similar to ID, indicating that axial conductivity enhanced contrasts in thermographs.

Sample TWC_09 featured an ID of 20.96% which is higher than that of sample TWC_08 but smaller than its AD at 25.9 ± 1.4 %; this shows an influence of multiple defects within a sample. Even though TWC_09 featured 1- and 2-yarn defects that were not identified individually, the MATLAB code was able to identify and quantify a correspondent area. This was not featured with sample STG_09, where only the largest 3-yarn defect was identified featuring a smaller ID than sample STG_06 featuring a 1-yarn defect. The influence of multiple defects was also present in sample USC_10, for which the MATLAB code identified a lower signal from the two smallest ½-yarn and 1- yarn defects. In addition, C_t CMs were able to remove noise from stitch lines in USC samples, showing that different textiles may require different approaches in order to eliminate textile patterns.

5 CONCLUSION

This work demonstrates an initial approach towards the identification and quantification of defects in dry preforms, applying thermography as a non-destructive method for the inspection of carbon and glass fibre preforms. Three major factors were investigated: textile pattern, thermal conductivity, and lay-up sequence. The work shows that characterization of defects is governed by multiple variables defined at both macro- and micro-scales. In order to generate a deeper understanding, modelling of heat transfer by finite elements and a larger library of experimental data are recommended. From an economical and environmental perspective, IR inspection can reduce rejection rates for composite parts, and potentially assist automation of lay-up systems and support

characterization of recycled CF and GF preforms [22,23]. Therefore, further work will be conducted to refine the technique since the authors acknowledge the use of simple experimental settings and algorithms in this work.

6 REFERENCES

1. A. A. Khatibi, H. R. Maleki, *Polymer Composites*, **29**, 7 (2008).
2. B. Bernberg. *Liquid Composite Molding achieves aerospace quality*, *High-performance Composites*, (2003).
3. M. S. Rao, *Composite Materials and Processes for civil aircraft structures*, (2007).
4. A. B. Strong, *Fundamentals of Composites Manufacturing: materials, methods and applications*, SME, Dearborn, Michigan (2008).
5. Z. Zhang, M. Sarhadi, *J. Materials Processing Technology*, **61**, (1996).
6. M. Pener, S. Algermissen, R. Keimer, H. P. Monner, *Robotic and Computer Integrated Manufacturing*, **38**, (2016).
7. S. Zhu, C. Magnussen, E. Judd, M. Frank, F. Peters, *J. of Manufacturing Science and Engineering*, **139**, (2017).
8. P. Cawley, Inspection of Composites – Current Status and Challenges, *ECNDT*, **Mo. 2.6.1** , (2006).
9. X. Madalque, *Nondestructive Evaluation of Materials by Infrared Thermography*, Springer-Verlag London. Université Laval, Quebec (1993).
10. H. Zhang, L. Yu, U. Hassler, H. Fernandes, M. Genest, F. Robitaille, S. Joncas, W. Holub, Y. Sheng, X. Madalque. *Composites Science and Technology*, **126**, (2016).
11. D. Balageas, X. Madalque, D. Burleigh, V. P. Vavilov, B. Oswald-Tranta, J.-M. Roche, C. Pradere, G. M. Carlomagno, *Thermal (IR) and Other NDT Techniques for Improved Material Inspection*, *J. Nondestructive Evaluation*, (2016).
12. C. J. Fiedler, *AIP Conf. Proc.*, **557**, 308 (2001).
13. X. Madalque, *Theory and Practice of Infrared Technology for Nondestructive Testing*, John Wiley & Sons. Université Laval, Quebec (2001).
14. U. Polimeno, D. P. Almond, B. Weekes, E. W. J. Chen, *Composites: Part B*, **59**, (2014).
15. <http://www.azom.com/properties.aspx?ArticleID=764>
16. <http://www.matweb.com/search/datasheet.aspx?matguid=d9c18047c49147a2a7c0b0bb1743e812&ckck=1>
17. D. Bigaud, J. M. Goyh  neche, P. Hamelin, *Composites Part A: Applied Science and Manufacturing*, **32** , (2001).
18. S. Hind, F. Robitaille, *Polymer Composites*, **31**, (2010).
19. Y. Yang, F. Robitaille, S. Hind, *Thermal Conductivity of Carbon Fiber Fabrics*, (2013).
20. Y. Yang, MSc thesis, University of Ottawa, (2013).
21. N. Bol'shakova, O. Kostenok, A. Il'in, V. Kostyukhin, *Plenum Publishing Corporation*, (1991).
22. I. Okajima, K. Watanabe, S. Haramiishi, M. Nakamura, Y. Shimamura, T. Sako, *J. of Supercritical Fluids*, **119**, (2017).
23. C. Morin, A. Loppinet-Serani, F. Cansell, C. Aymonier, *J. of Supercritical Fluids*, **66**, (2012).